Contents lists available at ScienceDirect

Colloids and Surfaces A: Physicochemical and Engineering Aspects

Three scenarios of freezing of liquid marbles

Anton Starostin [a], Vladimir Strelnikov [a], Leonid A. Dombrovsky [b,c,d], Shraga Shoval [e], Edward Bormashenko [e,*]

[a] Institute of Technical Chemistry, Academician Korolev St., 3, Perm 614013, Russia
[b] Department of Industrial Engineering and Management, Faculty of Engineering, Ariel University, P.O.B. 3, 407000 Ariel, Israel
[c] X-BIO Institute, University of Tyumen, 6 Volodarskogo St, Tyumen 625003, Russia
[d] Heat Transfer Department, Joint Institute for High Temperatures, 17A Krasnokazarmennaya St, Moscow 111116, Russia
[e] Chemical Engineering Department, Faculty of Engineering, Ariel University, P.O.B. 3, 407000 Ariel, Israel

HIGHLIGHTS

- Freezing of water marbles coated with various powders was studied.
- Various pathways of freezing were registered.
- The mathematical model of freezing is suggested.
- Qualitative analysis of marbles' deformation under cooling is supplied.
- De-pinning of the contact line governs the eventual shape of frozen marbles.

GRAPHICAL ABSTRACT

Main scenarios of freezing of liquid marbles
conical tip   spherical marble   flattened marble
1 mm   1 mm   1 mm
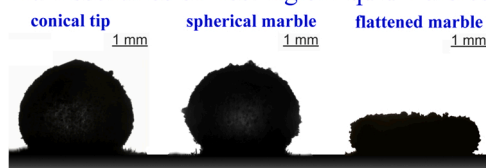
ARTICLE INFO

ABSTRACT

Controlled freezing of water marbles coated with various hydrophobic powders was studied in situ. Three main pathways of freezing were registered, namely: i) freezing accompanied with the formation of the conical "freezing tip" singularity; ii) freezing keeping the initial spherical shape of the marble; iii) freezing resulting in the formation of flattened axisymmetric crystallized puddles. The mathematical model of freezing is reported. Qualitative analysis of marbles' deformation under cooling is supplied. The effective surface tension of the studied water marbles is established experimentally. Thermal and elastic properties of water marbles, which are close for the studied marbles, are not responsible for the observed diversity of the freezing pathways. De-pinning of the contact line governs to the much extent the eventual shape of the frozen water marble. Strong pinning of the contact line promotes the formation of the "freezing tip singularity"; whereas, weak pinning results in the formation of flattened, oblate spheroid-like eventual shapes of the frozen water marbles.

1. Introduction

One of the most fascinating phenomena emerging from the intersection of the interface science and fluid mechanics is generation of singular structures and interfacial flows [1–6]. One of such singularities arises from the problem of the moving three-phase contact line. It is known that classical hydrodynamic description of the moving contact line leads to a non-integrable stress singularity [2,3]. Another type of singularity stems from the viscous motion of fluid with a free surface. The flow field analysis based on Navier-Stokes equations showed a singularity as the height of the fluid neck goes to zero [4]. Singularities of the water strider interfacial propulsion mechanisms were addressed recently in ref. [5]. The known singularity is observed under formation of the Taylor cone, observed when a jet of charged particles emanates

from the liquid/vapor interface above a threshold voltage [7,8].

Surface tension of water tends to oppose the formation of the aforementioned singularities, usually surface tension does not like sharp points, as mentioned in ref. [1]. Usually, the driving force responsible for the singularity is balanced by the surface tension on a scale that is much smaller than the scale of the flow; thus, it is quite challenging to observe singularities experimentally. We address in our research the freezing of non-stick water drops, providing a simple example of the formation of a cusped singularity (also labeled "pointy" ice drop formation) that is simple to reproduce and study [1,9–13]. Universality of the conical tip shape appearing at the apex of the freezing droplets was addressed in refs. [9,12]. It was demonstrated experimentally, that the cone angle is independent of substrate temperature and wetting angle, hinting to an universal physical mechanism which is independent of the rate of solidification [9,11,12]. The role of gravity in formation of the resulting shape of freezing droplet was clarified in ref. [11]. Influence of the impurities on the formation of the "freezing tip" was studied in ref. [13]. It was recently reported that a conical tip may be broken down due to the presence of nanoparticles; instead, the top of a frozen nanofluid droplet exhibits a flat plateau shape and such a plateau becomes larger at higher particle concentrations [14].

Freezing and re-melting of liquid marbles, giving rise to the formation of the conical tip, was investigated in ref. [15]. Liquid marbles, studied in the pioneering paper by Quéré et al. [19], are non-stick water droplets coated with nano- or micron-sized particles, which are usually hydrophobic [17–35]. Liquid marbles, which have been subjected to intensive research recently, demonstrate a diversity of fascinating properties; in particular, they enable transport of reactive fluids [17]. Liquid marbles respond to the surrounding gases and "breath" [19,25]. This made possible bio-medical applications of liquid marbles such as mini-bio-reactors and mini-reservoirs for cells cultivation [19,21,22]. Liquid marbles allow numerous microfluidics applications [18,20,28]. The Belousov–Zhabotinsky reaction carried out in liquid marbles was also demonstrated [31,32]. Liquid marbles also pose the fundamental problems of the interface science, in particular the problem of their conventional effective surface tension was intensively debated [26,27]. We address in our investigation crystallization of liquid marbles and

demonstrate that three various eventual shapes emerge from freezing, depending on the coating of a liquid marble and its adhesion to the cooled substrate. Pointy ice marble formation is not the only possible pathway of freezing. Somewhat surprisingly, we observed formation of the oblate-spheroid-shaped marbles under their freezing.

2. Materials and methods

2.1. Materials

For manufacturing of liquid marbles we used three kinds of powders, namely: Urchin-like particles based on aluminum oxide (SEM images are shown in Fig. 1**A**).

Silicon dioxide (Aerosil 380, supplied by Avonik Germany, the specific area $\widetilde{s} = 380 m^2 g^{-1}$, (SEM images are shown in Fig. 1**B**); Silicon dioxide (Newsil 125, China, the specific area $\widetilde{s} = 125 m^2 g^{-1}$, supplied by the Wu Xi queue Chen Silicon Chemical Co. Ltd), (SEM images are shown in Fig. 1**C**).

Powders were coated with H,1H,2H,2H-perfluorodecyltrichlorosilane (abbreviated FDTS), labeled *F*-coating (fluorinated coating) and n-Decyltriethoxysilane (abbreviated DTES) labeled correspondingly *S*-coating (silanized coating). Thus, "powder 1F" means the urchin-like particles coated with FDTS, powder 1S means respectively the urchin-like particles coated with DTES, etc., as summarized in Table 1. When we speak about the "urchin-like particles" we

Table 1
Powders used for the manufacturing of liquid marbles and scenarios of their freezing.

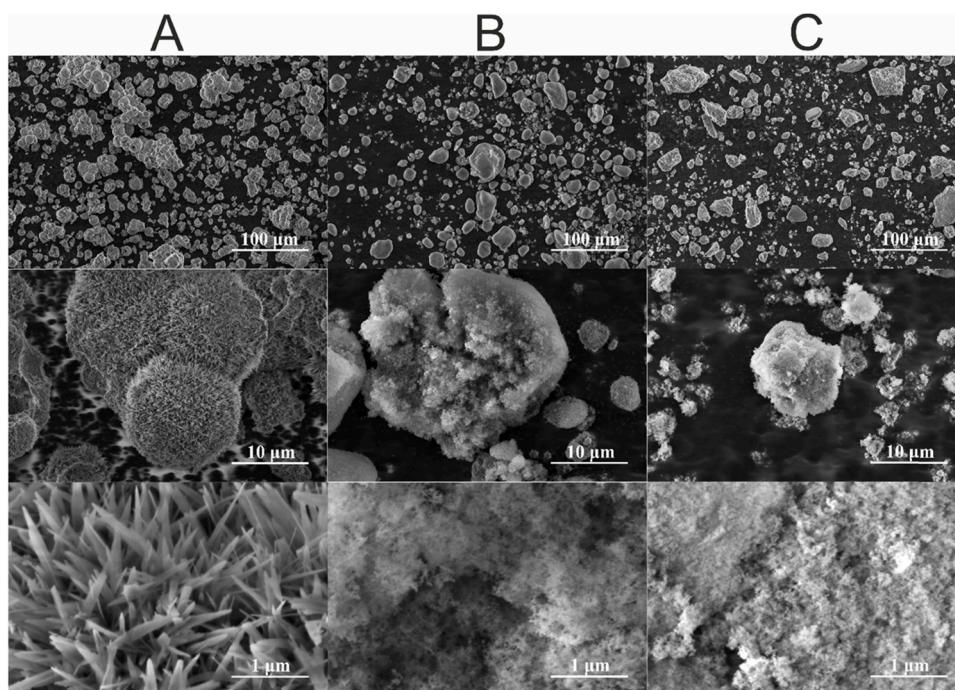| Powder	Coating	Labeling	Freezing Scenario
Urchin-like particles	FDTS	1F	III
Urchin-like particles	DTES	1S	I
Silicon dioxide (Aerosil 380)	FDTS	2F	II
Silicon dioxide (Aerosil 380)	DTES	2S	II
Silicon dioxide (Newsil 125)	FDTS	3F	III
Silicon dioxide (Newsil 125)	DTES	3S	I

Fig. 1. SEM images of the powders used in the investigation. A) Urchin-like particles based on aluminum oxide; B) Silicon dioxide powder (Aerosil 380); C) Silicon dioxide powder (Newsil 125).

mean particles coated with the aluminum oxide needles, such as shown in Fig. 1A. Both of fluorinated and silanized coatings supplied pronounced hydrophobic properties to the powders, as shown in Fig. 2.

Urchin-like hydrophobic particles, shown in Fig. 1A, were obtained by the method of hydrothermal synthesis, from an aqueous-alcoholic solution of aluminum salts taken at a ratio of $Al_2(SO_4)_3$: $Al(NO_3)_3$ = 80: 20 ml% / mol%. The molar ratios of the components of the synthesis were Al^{3+}/ $CO(NH_2)_2$/ H_2O/ i-PrOH = 1: 2: 100: 5, the synthesis scheme is described in detail in ref. [36]. The average diameter of the spherules was 10 ± 1 μm. Aluminum nitrate was supplied by Sigma-Aldrich, 2-propanol 98%, Urea 99% were supplied by Acros Organics.

It should be emphasized, that all of the investigated powders are inherently hydrophilic and cannot be used for manufacturing of liquid marbles; they form stable water suspensions. In order to prepare liquid marbles the powders were hydrophobized as follows: at the first stage of the process 0.4 g of FDTS or DTES were introduced into 50 ml of hexane. 4.0 g of the particles were introduced into the solution under the mixing concentration of 7.5%. The suspension was homogenized with the ultrasonic disperser Bandelin Sonopuls HD 3200 (module KE 76) during two minutes. Afterwards, these particles were dried under $t = 50^oC$ during 3 h and finally annealed under the temperature of 150 °C during 1 h. The manufactured hydrophobized urchin-like Al_2O_3 particles were used for manufacturing of the icephobic, omniphobic coating, as demonstrated in ref. [37]. Double-distilled water was used as a liquid. Specific conductivity of water was $\hat{\rho} = 3.8 \pm 0.1 M\Omega \times cm$ at the temperature of $t = 25^0C$.

2.2. Methods

2.2.1. Manufacturing of liquid marbles

10 μl liquid marbles filled with the bi-distilled water and coated with three kinds of powders listed in Section 2.1 were prepared. Aforementioned powders (see Section 2.1) were spread uniformly on a super-hydrophobic surface. Water droplets with the volume of $V = 10 \mu l$ were deposited using a precise micro-syringe on the powder layers; Rolling of the droplets resulted in the formation of liquid marbles enwrapped with the aforementioned hydrophobic powders, as shown in Fig. 3.

2.2.2. Freezing of liquid marbles and the temperature control under freezing

The marble was placed on the hydrophobic surface of the thermo-electric module and the change in the shape of the marble during the droplet cooling and crystallization was recorded using video filming, as shown in Fig. 4. Change in the shape of marbles in a course of their cooling and crystallization was monitored with the digital video camera

with a resolution of 1920×1200 pixel.

Cooling liquid marbles from $t = 12 \pm 0.5^0C$ to $- 12 \pm 0.5$ °C was performed with the thermo-electric modulus with a power of W = 95 W, enabling the maximal temperature change of 84 °C. The cooling rate was 20 ± 1 °C/min. Cooling was performed with the thermo-electric modulus under circulation of refrigerant trough the copper heat exchanger. The surface temperature was controlled with the dual laser IR sensor and the K-type thermocouple. Initial temperature and relative humidity (RH) in the experimental cell were set as $t = 25 \pm 0.5$ °C; RH = $40 \pm 1\%$. The testing was carried out with the experimental cell described in Fig. 4. Geometrical parameters of the cell are supplied in Fig. 4.

An accurate temperature control is of a primary importance of the experimental data. The temperature control within the cooled working cell was carried out with a pair of thermocouples: the first one measured the surface temperature of the cold plate, and the second one controlled the air temperature at the distance of 3 mm from the surface.

The details of the temperature control are addressed in detail in Appendix A.

2.2.3. Measurement of the effective surface tension of liquid marbles

The effective surface tension of liquid marbles was established with the "maximal marble height" method (also mentioned in the literature as the "maximal puddle height method") suggested in ref. [38] and developed in refs. [39–42]. The maximum height of the liquid marble was determined using a laboratory goniometer (CRUSS DSA-100, GmbH) with the software CRUSS ADVANCE. The volume of water in liquid marble was gradually increased to 1000 μl and the maximum (saturation) height of the puddle was taken, as shown in Fig. 5. The effective surface tension of the studied marbles was calculated using Eq. (1).

$$\gamma_{\text{eff}} = \frac{\rho g H_{max}^2}{4 sin^2 \left(\frac{\theta}{2} \right)} \quad , \tag{1}$$

where $H_{\max}$ is the maximal height of a puddle (see Fig. 5), γ_{eff} is the effective surface tension of the marble–air interface (i.e. the effective surface tension of the marble), ρ is the density of water, and θ is the apparent contact angle of the marble, depicted in Fig. 5. Effective surface tensions of the studied liquid marbles are summarized in Table 2.

2.2.4. Monitoring of the shape of the frozen water marbles and measurement of the contact area during crystallization

Continuous monitoring of the shape of the frozen liquid marbles was carried out with the digital camera and it is illustrated in Fig. 6. The
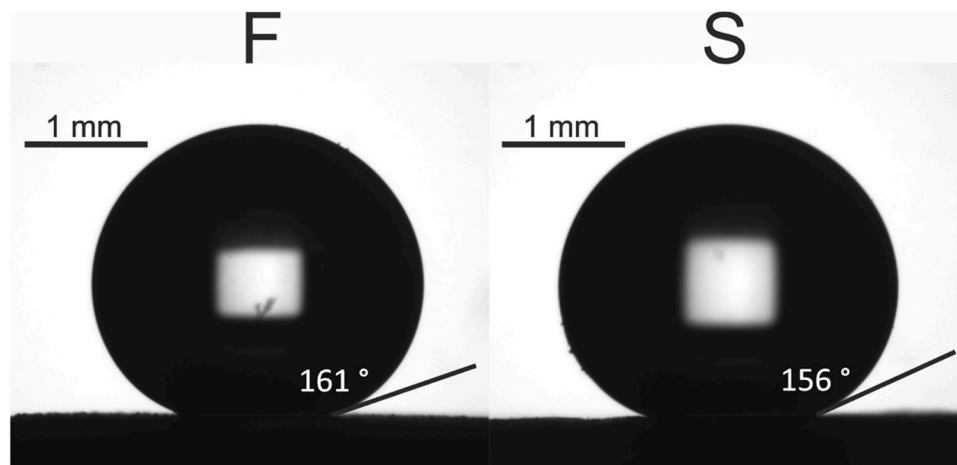

Fig. 2. Apparent contact angles of the fluorinated (left) and silanized (right) urchin-like particles based on aluminum oxide are depicted. $10 \mu l$ water droplet is placed on the powders. Scale bar is 1 mm.
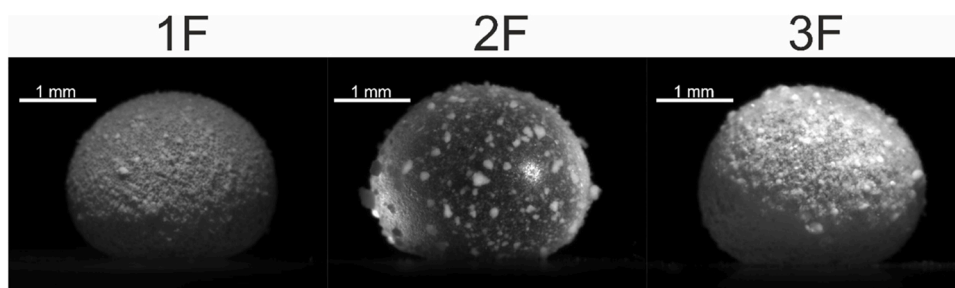
Fig. 3. Images of the liquid marbles used in the investigation are presented. The coating powders are: 1F) Fluorinated urchin-like particles based on aluminum oxide; 2F) Fluorinated silicon dioxide powder (Aerosil 380); 3F) Fluorinated silicon dioxide powder (Newsil 125). Scale bar is 1 mm.
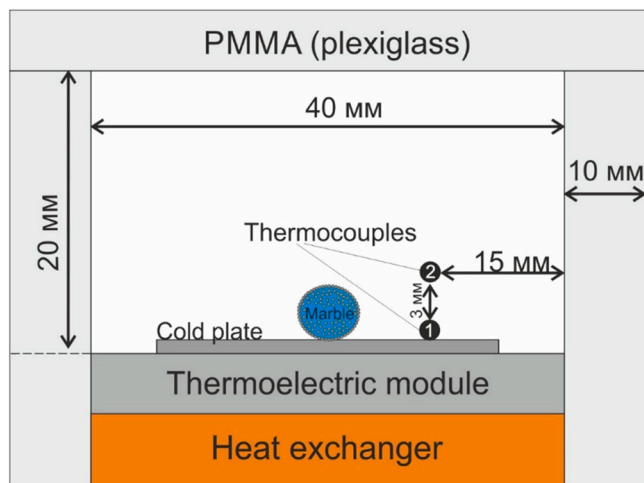

Fig. 4. Scheme of the experimental cell is depicted.

measurement of the contact radii of the cooled marbles was carried out in situ with the frozen marbles imaged using the laboratory goniometer. The contact radius of liquid marbles grew under cooling, as shown in Fig. 7. The diameter of the triple line was estimated with the KRUSS ADVANCE software as shown in Fig. 7. The results obtained for different marbles are presented in Table 3. Monitoring of the freezing enabled estimation of the velocity of crystallization front within a marble.

3. Results and discussion

3.1. Experimental observations

The total time of crystallization τ_{cr} was established with imaging (see Section 2.2.2 and Fig. 4) as $\tau_{cr} \cong 20-25$s for the marbles labeled 1F, 1S, 2F, 2S and $\tau_{cr} \cong 15-20$s for the marbles labeled 3F-3S. Thus, we conclude that the total time span of crystallization was close for all kinds of the studied hydrophobic coatings and only slightly dependent on the specific coating,

Three very different pathways (scenarios) were observed under freezing of the studied liquid marbles, namely: formation of typical "freezing tip" singularity, shown in Fig. 6**A** (labeled "scenario I), formation of the spherical frozen marbles, keeping their initial shape, depicted in Fig. 6**B** (denoted "scenario II) and formation of "flattened marbles" (labeled scenario III) illustrated in Fig. 6**C**. Formation of the marbles crowned with the freezing tip and flattened marbles is illustrated with the **Supplementary Video 1**. The singular freezing tips well-known to investigators were observed when 1S and 3S liquid marbles were cooled. The opening angle of the cone tip was established as $\alpha \cong 135-140^0$ (as shown in Fig. 7) and it was independent of the kind of coating. This value is very close to that reported by other research groups (see refs. [9,10,12]). This finding supports the idea that the
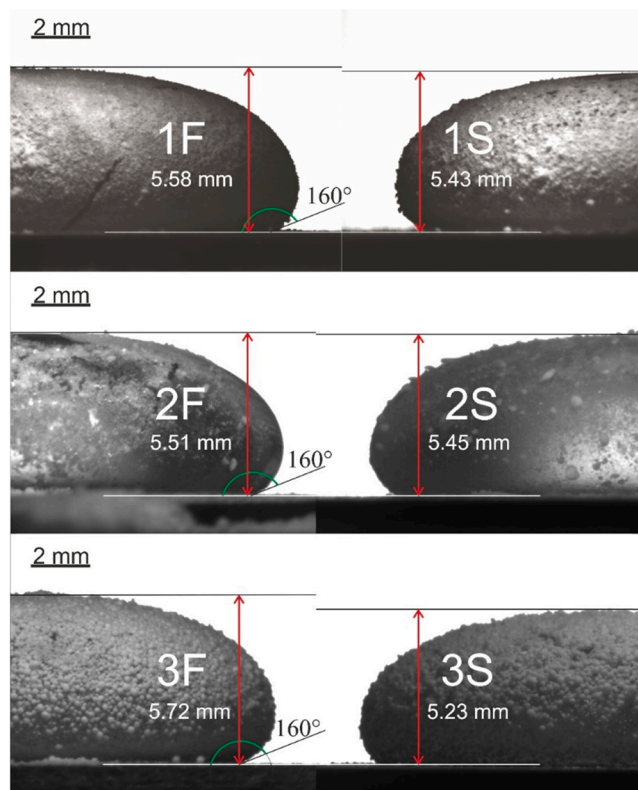

Fig. 5. Establishment of the effective surface tension of the marbles with the "maximal puddle height" method is depicted. The maximal (saturation) height and the apparent contact angles are shown for various types of marbles. Scale bar is 2 mm.

formation of the tip is due to the fact, that the density of ice is lower than the density of water [9–12]. Thus, the physical mechanism of formation of the freezing tip is universal and independent of the interfacial properties of the frozen liquid [9–12]. However, the eventual shaping of the frozen marble is not universal, and it depends strongly on the adhesion between the coating powder and the cooled solid substrate, as it will be shown below.

Supplementary material related to this article can be found online at doi:10.1016/j.colsurfa.2021.128125.

Formation of spherical crystallized droplets (scenario II) were inherent for the marbles coated with the spherical Aerosil 380 silicone dioxide nanoparticles coated with FDTS (powder 2F), as shown in Fig. 6**B**. Urchin-like particles and silicon dioxide Newsil 125 coated with FDTS gave rise to flattened droplets (scenario III) when cooled as shown in Fig. 6**C**. The experimental results are summarized in Table 1. Actually pathway II is an intermediate one between pathways I and III.

What is the physical reasoning explaining the difference in the

Table 2

Values of effective surface tension of the liquid marbles.

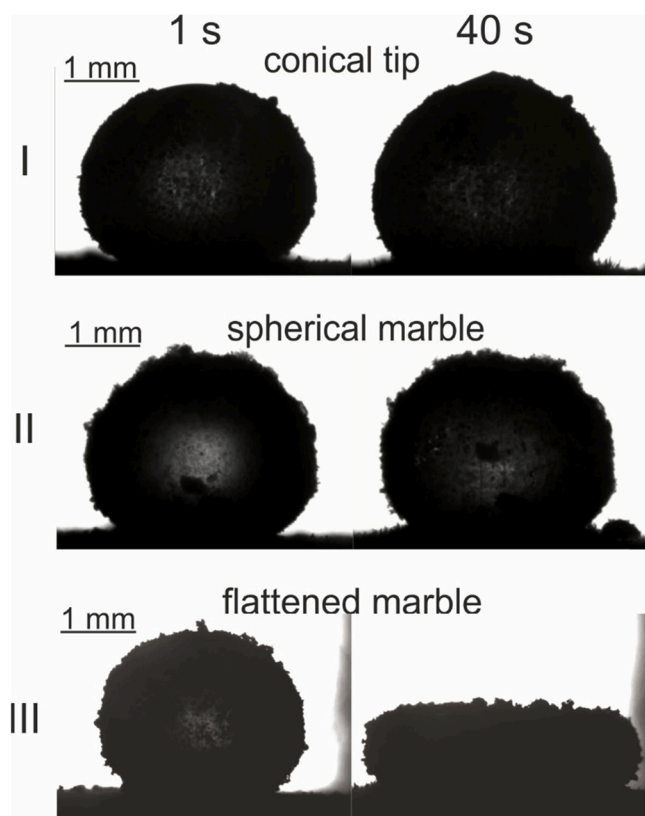| Powder	Coating	Labeling	Puddle volume, μl	H_{max}, mm	θ, °	γ, mJ/m^2
Urchin-like particles	FDTS	1F	1000 ± 5	5.6 ± 0.1	160 ± 2	75.4 ± 2
Urchin-like particles	DTES	1S		5.4 ± 0.1		71.4 ± 2
Silicon dioxide (Aerosil 380)	FDTS	2F		5.5 ± 0.1		73.5 ± 2
Silicon dioxide (Aerosil 380)	DTES	2S		5.5 ± 0.1		71.9 ± 2
Silicon dioxide (Newsil 125)	FDTS	3F		5.7 ± 0.1		79.2 ± 2
Silicon dioxide (Newsil 125)	DTES	3S		5.2 ± 0.1		66.2 ± 2

Fig. 6. Pristine liquid marbles (left column) and crystallized marbles (right column) are shown. Three main scenarios of freezing of liquid marbles are demonstrated: I) Formation of a conical tip (Scenario I); II) Formation of a spherical crystallized marble (Scenario II); III) Formation of the flattened crystallized marble (Scenario III). Scale bar is 1 mm.

Fig. 7. Change in the radius of the triple line for freezing water marble coated with various powders. The freezing tip angle is shown for 1S and 3S marbles. The right column (taken at $t = 40s$) corresponds to the complete freezing of the marbles. Scale bar is 1 mm.

aforementioned scenarios of freezing of liquid marbles? Three main physical factors may be responsible for this difference, namely:

i) difference in the freezing process itself due to the various thermo-physical properties of the liquid marbles;
ii) difference in the interfacial and elastic properties of the liquid marbles due to the physical properties of the coating powders;
iii) difference in the interfacial contact occurring between the marbles and the cooled surface.

We address consequently these groups of physical reasons below.

3.2. The thermal model of the initial stage of marble solidification

Consider the initial stage of freezing the marble. Strictly speaking, the correct calculation of water crystallization in the marble should account for the latent heat of the phase change. Fortunately, a contribution of the latent heat to the transient thermal state of the marble is negligible because of a relatively low initial velocity of the crystalliza-
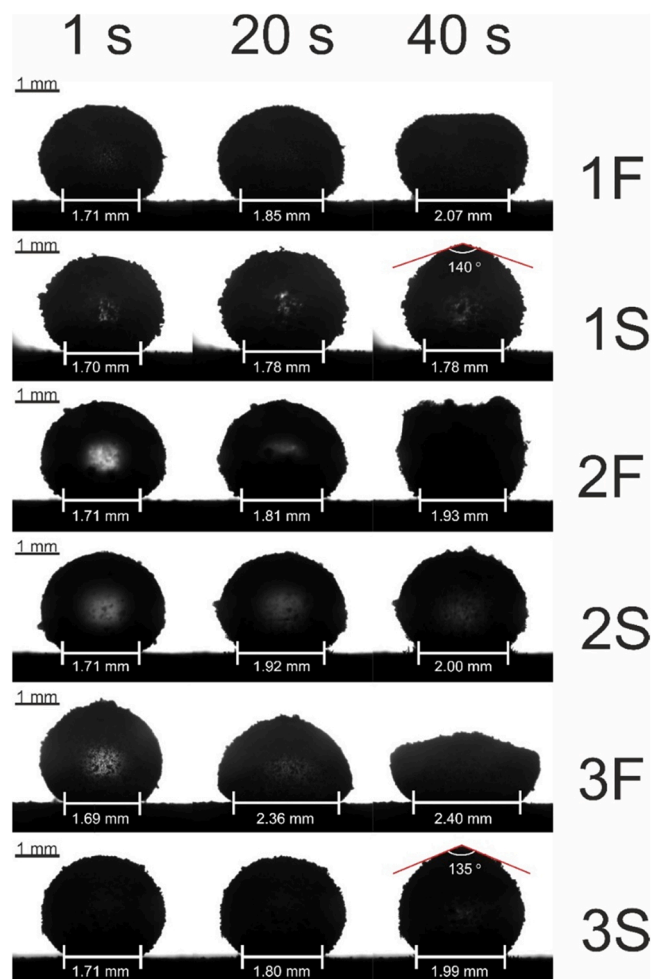
tion front (this will be shown below). Therefore, the problem is reduced to the ordinary transient axisymmetric heat conduction equation:

$$\rho c \frac{\partial T}{\partial t} = \frac{\partial}{\partial x}\left(k\frac{\partial T}{\partial x}\right) + \frac{1}{r}\frac{\partial}{\partial r}\left(k\frac{\partial T}{\partial r}\right) \qquad (2)$$

where x is the axial coordinate measured from the marble bottom and r is the radial coordinate measured from the vertical axis of symmetry, ρ, c, and k are the averaged density, heat capacity (per unit mass), and thermal conductivity of the medium, respectively; consider that the thermal properties of the cooled marbles are not uniform in the marble volume, which includes water, ice, and the coating. Note that this approximate thermal model ignores possible ice particles suspended in water and the thermal effect of motion of these particles in the convective flows of water. Eq. (2) should be accompanied by the initial

Table 3
De-pining of the triple line under crystallization.

Powder	Coating	Labeling	De-pinning Parameter, $\xi = \dfrac{\Delta r}{r_0}$
Urchin-like particles	FDTS	1F	0.21
Urchin-like particles	DTES	1S	0.047
Silicon dioxide (Aerosil 380)	FDTS	2F	0.13
Silicon dioxide (Aerosil 380)	DTES	2S	0.17
Silicon dioxide (Newsil 125)	FDTS	3F	0.84
Silicon dioxide (Newsil 125)	DTES	3S	0.16

condition and the boundary conditions to obtain a complete parabolic problem. These conditions can be estimated using the actual temperature measurements presented in Fig. 8. The initial temperature of the marble is assumed to be uniform and equal to the initial temperature of the cold plate:

$$T(0, x, r) = T_0 \qquad (3)$$

A parabolic extrapolation of the *Curve 1* depicting in Fig. 8 the temperature of the cold plate yields $T_0 = 12.8\ °C$. Due to the stable temperature stratification of air under the marble, it can be assumed, as it was done in ref. [43], that the heat conduction is the only mode of heat transfer from the lower surface of the marble to the cooled isothermal metal plate. It means that the heat transfer coefficient at the marble surface can be estimated as:

$$h = k_{air}/\delta_x \qquad (4)$$

where $k_{air} = 0.023\,W/(m \times K)$ is the thermal conductivity of air and δ_x is the local distance (along the vertical axis of the marble) from the cold plate to the marble surface. The corresponding boundary condition of the third kind at the marble surface is:

$$k \quad \partial T/(\partial n) = h(T - T_{plate}) \qquad (5)$$

where $T_{plate}(t)$ is the measured temperature of the cold plate and $\vec{n}$ is the local outer normal to the marble surface.

To estimate heat transfer on the side and top surface of the marble, we need the to know the local air temperature, T_{air}, outside the thermal boundary layer. Approximate values of this temperature can be determined by line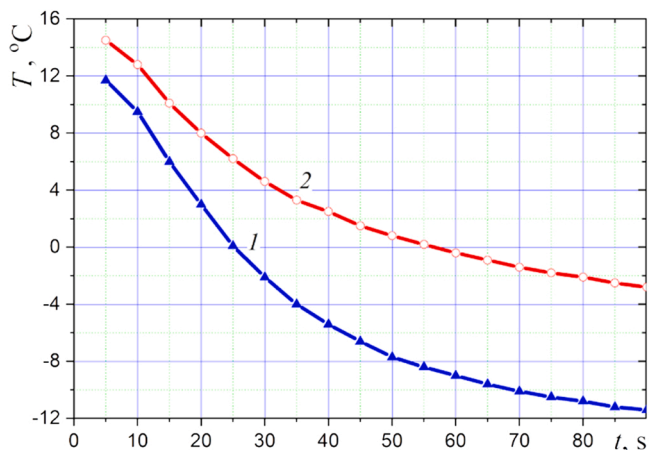ar interpolation between two measured temperatures: the temperature of the cold plate, T_{plate}, and the air temperature, $T_{air,H}$, at a height H above the plate:

$$T_{air}(t, x) = T_{plate}(t) + \left(T_{air,H} - T_{plate}\right)\frac{x}{H} \qquad (6)$$

Note that the temperature of air was measured at the height $H = 3$ mm, that is approximately equal to the initial diameter of the marble.

It is not a simple task to obtain the heat transfer coefficient, h, at both the side and upper surfaces of the marble. Therefore, we used estimations based on the limiting value of the Nusselt number $Nu = 2ah/k_{air} = 2$ for the slowly moving air and took into account the physical condition of continuous variation of the heat transfer coefficient along the marble surface. The details of the calculation of the thermal field in the cooled marble are supplied in Appendix B, using the approach reported in refs. [43–45]. Typical temperature field in the frozen marble is shown in Fig. 9. The calculated temperature profiles along the vertical axis of the marble at the initial stage of water crystallization are supplied in Fig. 10. The kinetics of upward propagation of a conventional crystallization front (i.e. the point $T = 0\ °C$) along the marble axis v_{fr} is illustrated with Fig. 11. It is seen that the velocity of propagation of the crystallization front grows with time, and at the final stage of the process (between 20 and 24 s of freezing) attains the value of $v_{fr} \cong 0.175\ \frac{mm}{s}$, which is in an excellent agreement with the experimentally established with imaging value $v_{fr} \cong 0.18\ \frac{mm}{s}$.

It should be emphasized that the temperature distribution predicted by the computational model is the same for all kinds of the marbles, and it could not explain the difference in the freezing scenarios, illustrated with Fig. 6. This is quite expectable due to the fact that the role of thermal properties of all the powders used for the marbles' manufacturing is insignificant.

Fig. 8. Time variation of temperature in the working cell: curve *1* – the temperature of the cold plate, curve *2* – the temperature of air at the height of 3 mm above the plate.
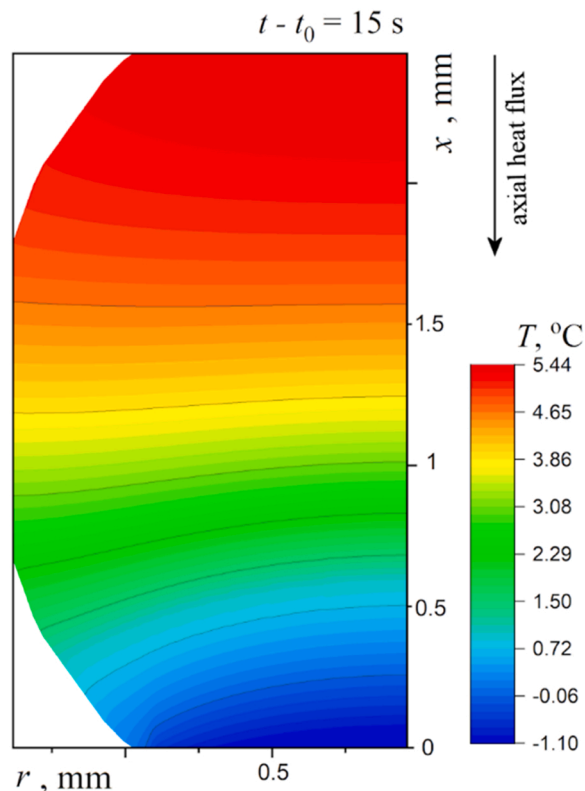

Fig. 9. Typical temperature field at the initial stage of the marble freezing is shown; x is the axial coordinate measured from the marble bottom and r is the radial coordinate measured from the vertical axis of symmetry.
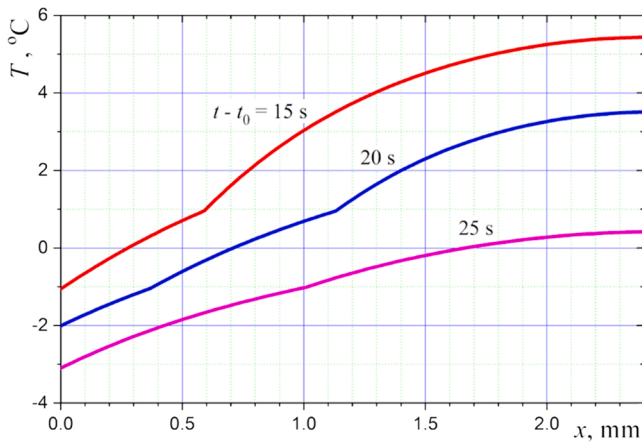
Fig. 10. Temperature profiles along the vertical axis of the marble at the initial stage of water crystallization are supplied.
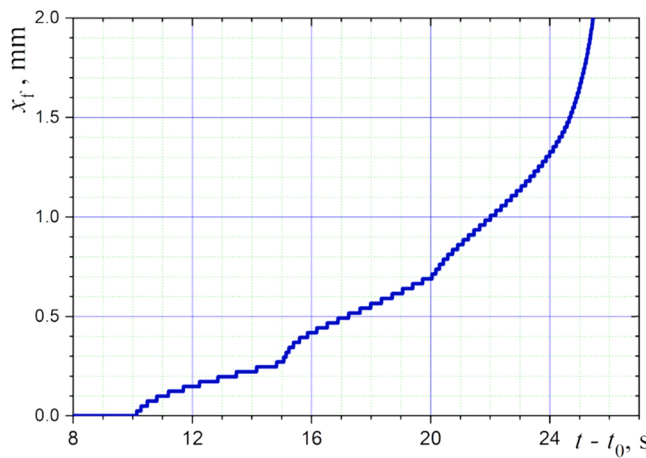

Fig. 11. Upward propagation of the point $T = 0$ °C (denoted x_f) along the marble axis is shown.

3.3. Analysis of the elastic stresses and deformation of the marbles under freezing

It is reasonable to assume that deformation of the frozen liquid marbles arises as the interplay of the gravity and thermal induced stresses [46–50]; thus, it will be useful to introduce the dimensionless parameter, defined as follows:

$$\Psi = \frac{\sigma_{th}}{\sigma_{gr}}, \tag{7}$$

where σ_{th} and σ_{gr} are stresses due to the thermal effects and gravity correspondingly. For the gravity-inspired stresses we reasonably adopt:

$$\sigma_{th} \cong \rho g R, \tag{8}$$

where ρ is the effective density of the marble which is very close to the density of water and R is the initial radius of the non-deformed marble. For the estimation of σ_{th} we involve the generalized Young law derived and experimentally tested for the liquid marbles [47]:

$$\sigma_{th} \cong \frac{4\gamma_{eff}}{R} \epsilon_{th}, \tag{9}$$

where γ_{eff} and ϵ_{th} are the effective surface tension and thermal strain

correspondingly; thus the effective modulus Young of the marble is estimated as $E_{eff} \cong \frac{4\gamma_{eff}}{R}$ and it depends on the effective surface tension and radius of the marble only [47]. The effective surface tension of the marbles was established with the "maximal puddle method" with Eq. (1) as described in detail in Section 2.2.3. The effective surface tensions for various coating powders are summarized in Table 2, and it recognized from the supplied data that the effective surface tension of the marbles in confined within a very narrow range, namely $\gamma_{eff} \cong 66 - 79 \frac{mJ}{m^2}$ (these results coincide with the findings reported by the other groups [38–42]).

The thermal strain ϵ_{th} is estimated as follows: the density of ice in the temperature range from -5 to -10 °C is about 918 kg/m³. This means that the coefficient of volumetric expansion in the transition from water to ice with the above temperature is equal to $\alpha = 0.072$, and the coefficient of linear expansion is $\alpha_1 = \alpha/3 = 0.024$. If the ice occupies the lower spherical segment of the marble, simple transformations give the following relative elongation of the marble coating layer in this segment:

$$\epsilon_{th} = \Delta l/l_0 = \alpha_1 \overline{h}_{ice}(1 - \overline{h}_{ice}/2)\overline{h}_{ice} = h_{ice}/a \leq 1 \tag{10}$$

where h_{ice} is the height of the segment. The value of ϵ_{th} increases monotonically with $\overline{h}_{ice}$ up to $\epsilon_{h,max} = \alpha_1/2$ at $\overline{h}_{ice} = 1$. In this case, the average relative elongation of the coating is: $\epsilon = \alpha_1/4 = 0.6\%$. Substitution of Eqs. (8)-(10) into Eq. (7) yields:

$$\Psi \cong \frac{4\gamma_{eff}\epsilon_{th}}{\rho g R^2} \cong \frac{4\gamma_{eff}\alpha_1\overline{h}\left(1 - \frac{\overline{h}}{2}\right)}{\rho g R^2} \tag{11}$$

Assuming $\epsilon_{th} \cong 6.0 \times 10^{-3}$, $\gamma_{eff} \cong 70 \times 10^{-3}\frac{N}{m}$, $\rho \cong 10^3 \ \frac{kg}{m^3}$ and $R \cong 1.0 \times 10^{-3}$m we estimate $\Psi \cong 0.17$. This means that the stresses due to the thermal effects and gravity are of the same order of magnitude; however, gravity-inspired stresses prevail on the thermal ones. It should be emphasized that the values of γ_{eff} are very close for different coating powders as it is recognized from the data supplied in Table 2. Thus, we conclude that the values of the dimensionless constant Ψ are also close for various marbles frozen in our study. Hence, the elastic properties of the studied marbles do not constitute the difference in the shaping of the marbles under their cooling, illustrated with Fig. 6.

3.4. Pinning of the contact line and its role in the shaping of the frozen marbles

We already concluded that thermal and elastic properties of the liquid marbles are hardly responsible for the dramatic difference in the shaping under freezing. The clue is locked in the behavior of the triple line under cooling of liquid marbles [51,52]. We established that some of the explored powders promoted strong pinning of the contact line to the substrate under freezing, whereas some of them provided distinct de-pinning of the contact line under cooling, as shown in Fig. 7. In order to quantify the effect of de-pinning it is instructive to introduce the dimensionless de-pinning parameter ξ defined according to Eq. (12):

$$\xi = \frac{r_f - r_0}{r_0} = \frac{\Delta r}{r_0}, \tag{12}$$

where r_0 and r_f are the initial and final radii of the contact line, shown in Fig. 7. The numerical values of the dimensionless de-pinning parameter ξ, as established experimentally, are supplied in Table 3. It is seen that, when the contact line of the marbles is strongly pinned under crystallization, the "freezing tip" singularity, corresponding to Scenario I of the process is observed (coating 1S and 3S), depicted in Fig. 6A. Strong pinning also may promote formation of the eventual spherical shape of the frozen marble (Scenario II, shown in Fig. 6B, coatings 2F and 2S). The value of the parameter ξ corresponding to Scenarios I and II is

$\xi \cong 0.047 - 0.17$. When the triple line is de-pinned under freezing (coatings 1F and 3F), Scenario III is realized and flattened, oblate spheroid shaped frozen marbles are observed (see Fig. 6C). This situation takes place under the high values of ξ, namely $\xi \cong 0.21 - 0.84$. Thus, we conclude that the effect of pinning of the triple line plays a crucial role on shaping of the frozen liquid marbles.

Most likely, this phenomenon of de-pinning of the triple line is constituted by two physical effects:

 i) formation of an ice layer in the lower part of the marble;
ii) adhesion of the coating powder to the cooled surface.

It is natural to assume that the horizontal expansion of the ice layer (the density of which is less than the density of water), when the diameter of this ice layer approaches the contact diameter of the marble, leads to tangential expansion of the marble coating, which gives rise to the de-pinning of the triple line. Consider the situation when the triple-line is de-pinned (Scenario III). The tensile stresses emerging from the tangential expansion of the marble are partially compensated by the elastic properties of the marble. With the simultaneous action of gravity, a moment comes when the easily deformable shell of the upper part of the marble (where water has not yet frozen) takes a shape, as if continuing the comparatively flatter lower part of the marble. Apparently, this is how an ice marble is obtained in the form of an oblate spheroid. The stronger adhesion of the coating powder to the cooled surface prevents the thermal expansion; in this situation (Scenario I) the traditional "freezing tip" is formed. Scenario II promoting formation of the spherical eventual marbles is intermediate between Scenarios I and II. The rigorous mathematical model of the process is desirable.

4. Conclusions

Adhesion of hydrophobic powders to the liquid/air interfaces is important for a variety of applications including mineral flotation [53], catalysis [54] and formation of liquid marbles. Liquid marbles are non-stick droplets coated with hydrophobic or moderately hydrophilic powders [16–25]. Such non-stick droplets were intensively studied in the last decade due to their potential for a diversity of microfluidic and biological applications [18–20]. We studied cooling of the liquid marbles coated with hydrophobized urchin-like particles based on alumina, and silica particles. We established that very different pathways of freezing of liquid marbles are possible, namely: i) cooling resulting in the formation of the crystallized marbles crowned with the "freezing tip" singularity, ii) freezing giving rise to the eventual spherical shapes, iii) freezing resulting in the formation of the flattened crystallized samples. The opening angle of the conical freezing tip was established as $\alpha \cong 135 - 140^0$, and it was independent of the kind of hydrophobic powder coating. This value is very close to that reported by other research groups and, thus, it hints to the universal nature of formation of this singularity discussed in refs. [9–14], and it is reasonably related to the difference in the densities of water and ice. We suggest the thermal model of the initial period of marbles' freezing. The model predicts accurately the experimentally established velocity of the motion of the crystallization front within the frozen marble. The model is universal for various marbles but does not supply an explanation for the diversity of the pathways of crystallization in the cooled marbles. We also report the effective surface tension of the studied marbles [38–42]. It turns out, that the effective surface tensions and Young moduli of all of the investigated marbles are very close one to another [46–50]. Thus, we conclude that neither thermal nor elastic properties of the liquid marbles are responsible for the difference in the pathways of their crystallization and eventual shaping. We related the diversity in the behavior of frozen water marbles to the effect of pinning of the contact line of the marbles [51,52], which may be strong or weak, depending on the adhesion of the coating powder to the cooled solid substrate. Strong pinning of the contact line promotes the formation of the freezing tip singularity, whereas, a weak pinning, in turn, gives rise to the formation of flattened eventual shapes of the crystallized water marbles. We conclude that various shapes emerge from the freezing of liquid marbles, depending on the effect of pinning of the contact line under cooling.

CRediT authorship contribution statement

Anton Starostin: Conceptualization, Formal analysis, Data curation, Investigation, Methodology, Validation, Visualization. **Vladimir Strelnikov:** Conceptualization, Investigation, Supervision, Project administration. **Leonid A. Dombrovsky:** Conceptualization, Data curation, Investigation, Methodology, Software. Writing – original draft, Writing – review & editing. **Shraga Shoval:** Conceptualization, Formal analysis, Data curation, Investigation, Methodology, Supervision, Writing – original draft, Writing – review & editing. **Edward Bormashenko:** Conceptualization, Investigation, Methodology, Validation, Writing – original draft, Writing – review & editing.

Declaration of Competing Interest

The authors declare that they have no known competing financial interests or personal relationships that could have appeared to influence the work reported in this paper.

Acknowledgements

Appendix A. Precise temperature control of marbles' freezing

See Appendix Fig. A1.

In fact, only the temperature of the thermocouple bead is measured. This temperature is systematically different from the plate temperature or the air temperature.

In a cell cooled from below, a stable temperature stratification of air takes place. This means that the air is almost immovable and the main source of the error in the temperature measurements is the heat supplied to the bead along the thermocouple wires. This error can be easily estimated theoretically, but the best way to do it is a comparison of the measurements using two thermocouples with the wires of different thickness. The results of such a comparison are presented in Fig. 1A. This figure shows the temperature measurements of a cold plate, but the thermocouple is not pressed against the surface of the plate. Therefore, the main source of measurement error (as for the thermocouple surrounded by air) is associated with the heat supplied along the thermocouple wires. One can see that the effect of diameter of the thermocouple wires is significant. The thermocouples with the wires of diameter 0.1 mm were used for the temperature measurements.
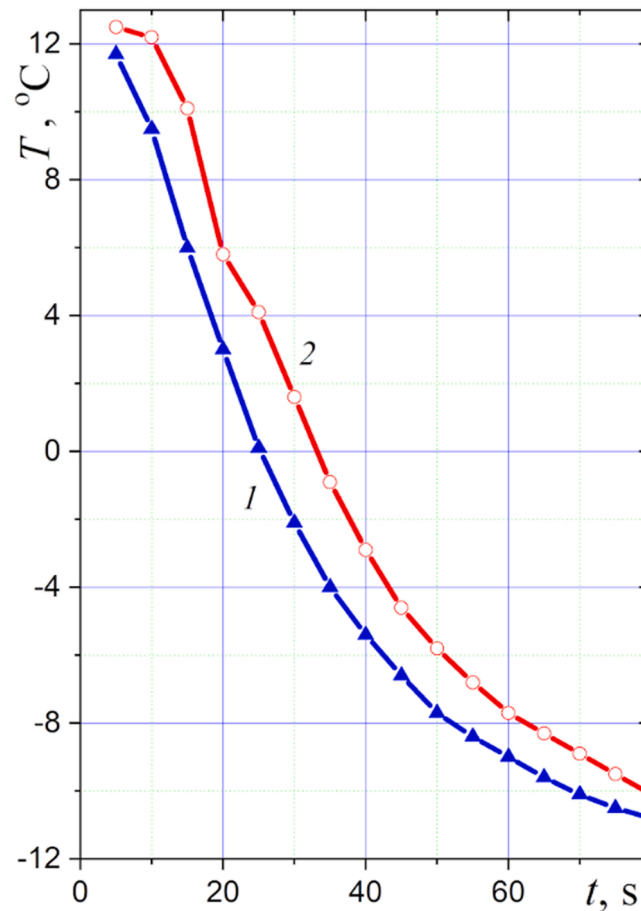
Fig. 1A. A typical comparison of temperature measurements using the thermocouples with wires of diameter 0.5 mm (*1*) and 0.1 mm (*2*).

Appendix B. Calculation of the thermal field in the frozen marble

The calculation of the thermal field in the frozen marble was carried out for the initial period of time when the deformation of the marble is insignificant. The radius of the spherical marble was taken to be $a = 1.46$ mm, including the coating thickness $\delta = 0.06$ mm. The volumetric heat capacity of water weakly depends on temperature, and this value was considered constant: $\rho_w c_w = 4.2$ MJ/(m^{3}K). On the other hand, the temperature dependence of the thermal conductivity coefficient should be taken into account. For this, we used the linear approximation:

$$k_w = 0.56 + 0.02 \times (273 - T) \tag{B1}$$

where the water temperature is measured in Kelvin, and the value of k_w is obtained in $\frac{W}{m \times K}$. For ice (at $T < 273$ K), the temperature dependence of both the volumetric heat capacity and the thermal conductivity coefficient should be taken into account:

$$\rho_{ice} c_{ice} \left[MJ / \left(m^3 K \right) \right] = 1.9 - 0.04 \times (273 - T[K]) \tag{B2}$$

$$k_{ice} [W/(m \times K)] = 2.2 + 0.02 \times (273 - T[K]) \tag{B3}$$

In the thin region of the phase transition (mushy zone), it was taken $\rho c \approx 3$ MJ/(m^3 K) and $k \approx 1.4 \frac{W}{m \times K}$. For the marble coating material, the following constant values of thermal properties were used: $\rho c = 4$ MJ/(m^3 K), $k = 2 \frac{W}{m \times K}$. Note that additional calculations showed a very weak effect of the coating on the cooling and freezing of water in the marble.

The heat conduction problem was solved using an implicit finite-difference scheme of the second order of approximation on an orthogonal grid with splitting the differential operator on the right side of Eq. (1) into two parts and alternately integrating the equation at each time step along a set of grid lines in the axial and radial directions. To use a simple rectangular grid with a constant step in both coordinates, the computational domain was simplified by cutting off the spherical protrusions. This slight distortion is just a technique that does not considerably affect the calculation results. The flat contact area with radius equal to 0.85 mm at the bottom of the marble was taken into account in the calculations. The numerical solution of the problem was carried out on a grid with 80 intervals along the radius and 100 intervals along the vertical axis of the marble. The time integration step was varied. Its minimum value is 0.01 s. Note that a similar computational procedure was used in solving diverse physical problems [1–3].

Before the numerical calculation, it is interesting to compare the velocities of heat propagation in water and air. Such a comparison can be based on the Fourier number:

$$\text{Fo} = \kappa t / d^2 \tag{B4}$$

where $\kappa = k/(\rho c)$ is the thermal diffusivity of the medium and d is the thickness of the medium layer. The condition Fo $= 1$ corresponds to the characteristic time of heating or cooling the layer. Obviously, the ratio of cooling time values for water and air layers of the same thickness can be written as follows:

$$t_\text{w}/t_\text{air} = \kappa_\text{air}/\kappa_\text{w} \tag{B5}$$

At temperature about 0 °C, the thermal diffusivities of these substances are: $\kappa_\text{air} = 1.88 \times 10^{-5}$ m^2/s and $\kappa_\text{w} = 1.32 \times 10^{-7}$ m^2/s, and Eq. (9) yields $t_\text{w}/t_\text{air} = 142$. This is sufficient to conclude that cooling of water in the marble is much slower than that of ambient air. As a result, a relatively cold air surrounding the upper part of the marble is an additional thermal factor which contribute to cooling and solidification of the marble. In addition, the thermal stratification of air at the top of the marble is unstable and this leads to a significant local intensification of convective cooling the marble. This effect was also taken into account in approximate numerical calculations.

Note that an accurate estimation of the time of the marble solidification is too complicated because of complex thermal conditions at the marble surface. The more or less reliable results can be obtained only on the basis of complex numerical analysis.

According to the measurements of the cold plate temperature shown in Fig. 8, the solidification of water in the marble is impossible at $t < t_0$, when the plate temperature is greater than 0 °C. Therefore, it is convenient to measure the time of solidification as a difference $t - t_0$. As to the vertical axial coordinate of the marble we use the difference $x - x_1$, where x_1 is the coordinate of the flat contact surface.

Some results of the numerical calculations are presented in Figs. 9–11. As was mentioned, these results are not accurate mainly due to uncertainty in the heat transfer conditions at the marble surface. However, the calculations show the character of the temperature field with a freezing zone near the marble bottom (Fig. 9), typical profiles of temperature along the marble axis (Fig. 10), and the upward propagation of a conventional front of crystallization (Fig. 11). Note that there is a qualitative agreement between the calculations for the initial stage of the marble freezing and the corresponding laboratory observations.

References

[1] J.H. Snoeijer, P. Brunet, Pointy ice-drops: How water freezes into a singular shape, Am. J. Phys. 80 (9) (2012) 764–771.
[2] L. Pismen, Mesoscopic hydrodynamics of contact line motion, Colloids Surf. A 206 (1–3) (2002) 11–30.
[3] L. Alexandrova, R. Koynova, L. Grigorov, B. Tenchov, Singular behavior of three-phase contact between DMPC dispersion, air and quartz at the critical temperature of 29°C, Colloids Surf. A 149 (1–3) (1999) 239–244.
[4] J. Eggers, Universal pinching of 3D axisymmetric free-surface flow, Phys. Rev. Lett. 71 (21) (1993) 3458–3460.
[5] Th Steinmann, A. Cribellier, J. Casas, Singularity of the water strider propulsion mechanisms, J. Fluid Mech. 915 (2021) A118.
[6] T.D. Blake, K.J. Ruschak, A maximum speed of wetting, Nature 282 (1979) 489–491.
[7] J.S. Eow, M. Ghadiri, The behaviour of a liquid–liquid interface and drop-interface coalescence under the influence of an electric field, Colloids Surf. A 215 (1–3) (2003) 101–123.
[8] J. Fernandez de la Mora, The fluid dynamics of Taylor cones, Annu. Rev. Fluid Mech. 39 (2007) 217–243.
[9] A.G. Marin, O.R. Enríquez, P. Brunet, P. Colinet, J.H. Snoeijer, Universality of tip singularity formation in freezing water drops, Phys. Rev. Lett. 113 (5) (2014), 054301.
[10] A. Schetnikov, V. Matiunin, V. Chernov, Conical shape of frozen water droplets, Am. J. Phys. 83 (1) (2015) 36–38.
[11] X. Zhang, X. Liu, J. Min, X. Wu, Shape variation and unique tip formation of a sessile water droplet during freezing, Appl. Therm. Eng. 147 (2019) 927–934.
[12] M.F. Ismail, P.R. Waghmare, Universality in freezing of an asymmetric drop, Appl. Phys. Lett. 109 (2016), 234105.
[13] F. Boulognea, A. Salonen, Drop freezing: fine detection of contaminants by measuring the tip angle, Appl. Phys. Lett. 116 (2020), 103701.
[14] Y. Zhao, C. Yang, P. Cheng, Freezing of a nanofluid droplet: from a pointy tip to flat plateau, Appl. Phys. Lett. 118 (201) (2021), 141602.
[15] D. Zang, K. Lin, W. Wang, Y. Gu, Y. Zhang, X. Geng, B.P. Binks, Tunable shape transformation of freezing liquid water marbles, Soft Matter 10 (9) (2014) 1309–1314.
[16] P. Aussillous, D. Quéré, Liquid marbles, Nature 411 (2001) 924–927.
[17] L. Harsha, T. Bhuyan, S. Maity, P. Mondal, S.S. Ghosh, D. Bandyopadhyay, Multifunctional liquid marbles to stabilize and transport reactive fluids, Soft Matter 17 (19) (2021) 5084–5095.
[18] C.H. Ooi, R. Vadivelu, J. Jin, K.R. Sreejith, P. Singh, N.-K. Nguyen, N.-Tr Nguyen, Liquid marble-based digital microfluidics – fundamentals and applications, Lab Chip 21 (7) (2021) 1199–1216.
[19] N.-K. Nguyen, C.H. Ooi, P. Singha, J. Jin, K.R. Sreejith, H.-P. Phan, N.-Tr Nguyen, Liquid marbles as miniature reactors for chemical and biological applications, Processes 8 (7) (2020) 793.
[20] C.H. Ooi, N.-Tr Nguyen, Manipulation of liquid marbles, Microfluid. Nanofluid. 19 (2015) 483–495.
[21] R.K. Vadivelu, H. Kamble, A. Munaz, N.-Tr Nguyen, Liquid marbles as bioreactors for the study of three-dimensional cell interactions, Biomed. Micro 19 (2) (2017) 31.
[22] S.M. Salehabad, S. Azizian, Sulfur liquid marbles submerged in biphasic systems as microreactors for interfacial synthesis, Colloids Surf. A 620 (2021), 126551.
[23] X. Li, Liquid marbles and liquid plasticines with nanoparticle monolayers, Adv. Colloid Interface Sci. 271 (2019), 101988.
[24] X. Li, H. Shi, Y. Wang, H. Wang, J. Huang, M. Duan, Liquid marbles from soot films, Soft Matter 16 (18) (2020) 4512–4519.
[25] E. Bormashenko, Liquid marbles, elastic nonstick droplets: from minireactors to self-propulsion, Langmuir 33 (2017) 663–669.
[26] E. Bormashenko, R. Pogreb, G. Whyman, A. Musin, Surface tension of liquid marbles, Colloids Surf. A 351 (2009) 78–82.
[27] E. Bormashenko, A. Musin, G. Whyman, Z. Barkay, A. Starostin, V. Valtsifer, V. Strelnikov, Revisiting the surface tension of liquid marbles: measurement of the effective surface tension of liquid marbles with the pendant marble method, Colloids Surf. A 425 (2013) 15–23.
[28] M. Uda, H. Kawashima, H. Mayama, T. Hirai, Y. Nakamura, S. Fujii, Locomotion of a nonaqueous liquid marble induced by near-infrared-light irradiation, Langmuir 37 (14) (2021) 4172–4182.
[29] Y. Asaumi, M. Rey, N. Vogel, Y. Nakamura, S. Fujii, Particle monolayer-stabilized light-sensitive liquid marbles from polypyrrole-coated microparticles, Langmuir 36 (10) (2020) 2695–2706.
[30] J. Fujiwara, F. Geyer, H.J. Butt, T. Hirai, Y. Nakamura, S. Fujii, Shape-designable polyhedral liquid marbles/plasticines stabilized with polymer plates, Adv. Mater. Interfaces 7 (24) (2020), 2001573.
[31] T.C. Fullarton, N. Draper, P.J. Phillips, B. de, L. Costello, A. Adamatzky, Belousov–Zhabotinsky reaction in liquid marbles, J. Phys.: Mater. 2 (1) (2019), 015005.
[32] A. Adamatzky, C. Fullarton, N. Phillips, B. de, L. Costello, T.C. Draper, Thermal switch of oscillation frequency in Belousov–Zhabotinsky liquid marbles, R. Soc. Open Sci. 6 (4) (2019), 190078.
[33] J. Saczek, X. Yao, V. Zivkovic, M. Mamlouk, D. Wang, S.S. Pramana, S. Wang, Long-lived liquid marbles for green applications, Adv. Funct. Mater. 31 (35) (2021), 2011198.
[34] B.T. Lobel, C.A. Thomas, P.M. Ireland, E.J. Wanless, G.B. Webber, Liquid marbles, formation and locomotion using external fields and forces, Adv. Powder Techn. 32 (6) (2021) 1823–1832.
[35] A. Gallo, F. Tavares, R. Das, H. Mishra, How particle–particle and liquid–particle interactions govern the fate of evaporating liquid marbles, Soft Matter 17 (33) (2021) 7628–7644.
[36] I.I. Lebedeva, A.S. Starostin, I.V. Valtsifer, V.A. Valtsifer, Hydrothermal synthesis of urchin-like alumina for fire-extinguishing powders, J. Mater. Sci. 53 (2018) 3915–3926.
[37] A. Starostin, V. Strelnikov, V. Valtsifer, I. Lebedeva, I. Legchenkova, E. Bormashenko, Robust icephobic coating based on the spiky fluorinated Al$_2$O$_3$ particles, Sci. Rep. 11 (2021) 5394.
[38] P. Aussillous, D. Quéré, Properties of liquid marbles, Proc. R. Soc. A 462 (2006) 973–999.
[39] P. Singha, C.-H. Ooi, N.K. Nguyen, K.R. Sreejith, J. Jin, N.-Tr Nguyen, Capillarity: revisiting the fundamentals of liquid marbles, Microfluid. Nanofluid. 24 (2020) 81.
[40] E. Bormashenko, R. Pogreb, G. Whyman, A. Musin, Colloids Surf. A Surf. Tens. Liq. Marbles 351 (2009) 78–82.
[41] E. Bormashenko, R. Pogreb, A. Musin, R. Balter, G. Whyman, D. Aurbach, Interfacial and conductive properties of liquid marbles coated with carbon black, Powder Technol. 203 (3) (2010) 529–533.
[42] R. Wang, X. Li, On the effective surface tension of powder-derived liquid marbles, Powder Technol. 367 (2020) 608–615.
[43] M. Frenkel, L.A. Dombrovsky, V. Multanen, V. Danchuk, I. Legchenkova, S. Shoval, Y. Bormashenko, B.P. Binks, E. Bormashenko, Self-propulsion of water-supported liquid marbles filled with sulfuric acid, J. Phys. Chem. B 122 (32) (2018) 7936–7942.
[44] L.A. Dombrovsky, V. Timchenko, C. Pathak, H. Piazena, W. Müller, M. Jackson, Radiative heating of superficial human tissues with the use of water-filtered

infrared-A radiation: a computational modeling, Int. J. Heat Mass Transf. 85 (2015) 311–320.

[45] A.A. Fedorets, L.A. Dombrovsky, Generation of levitating droplet clusters above the locally heated water surface: a thermal analysis of modified installation, Int. J. Heat Mass Transf. 104 (2017) 1268–1274.

[46] S. Asare-Asher, J.N. Connor, R. Sedev, Elasticity of liquid marbles, J. Colloid Interface Sci. 449 (2015) 341–346.

[47] G. Whyman, Bormashenko, interpretation of elasticity of liquid marbles, J. Colloid Interface Sci. 457 (2015) 148–151.

[48] H.-N. Polwaththe-Gallage, C.H. Ooi, J. Jin, E. Sauret, N.-Tr Nguyen, Z. Li, Y.T. Gu, The stress-strain relationship of liquid marbles under compression, Appl. Phys. Lett. 114 (2019), 043701.

[49] S. Azizian, S. Fujii, M. Kasahar, H.-J. Butte, M. Kappl, Effect of particle morphology on mechanical properties of liquid marbles, Adv. Powder Techn. 30 (2) (2019) 330–335.

[50] E. Bormashenko, R. Pogreb, R. Balter, H. Aharoni, Y. Bormashenko, R. Grynyov, L. Mashkevych, D. Aurbach, O. Gendelman, Elastic properties of liquid marbles, Colloid Polym. Sci. 293 (2015) 2157–2164.

[51] J. Liu, Y. Mei, R. Xia, A. New, Wetting mechanism based upon triple contact line pinning, Langmuir 27 (1) (2011) 196–200.

[52] S. Iliev, N. Pesheva, P. Iliev, Contact angle hysteresis on doubly periodic smooth rough surfaces in Wenzel's regime: The role of the contact line depinning mechanism, Phys. Rev. E 97 (2018), 042801.

[53] R. Crawford, J. Ralston, The influence of particle size and contact angle in mineral flotation, Int. J. Miner. Process. 23 (1–2) (1988) 1–24.

[54] F. Omota, A.C. Dimian, A. Bliek, Adhesion of solid particles to gas bubbles. Part 2: experimental, Chem. Eng. Sci. 61 (2) (2006) 835–844.